A 32-Gigahertz Coupled-Cavity Maser Design

J. S. Shell[1] and R. C. Clauss[2]

A 32-GHz coupled-cavity maser design is described. The theory and the predicted performance of cavity masers are included. A coupling cavity in the signal waveguide enables tuning of the maser over the 500-MHz-wide deep-space frequency allocation from 31.8 GHz to 32.3 GHz. The ruby cavity is simultaneously resonant at 32 GHz in the TE_{101} mode and at the pump frequency of 66.4 GHz in the TE_{301} mode. A pump rejection filter is incorporated to help confine the pump energy to the ruby and coupling cavities. A mode-matching analysis program was used to determine the dimensions and the tolerances for this design. Equivalent circuits using lumped elements showing characteristics of the cavities, filters, and ruby spin system were generated. A 3.1-K maser noise temperature in a 2.2-K cryogenic refrigerator is predicted at 32 GHz.

I. Introduction

The deep-space allocation for signals from space to Earth at Ka-band covers a 500-MHz frequency range extending from 31.8 GHz to 32.3 GHz. Reception of Ka-band signals from interplanetary distances, with typical power densities at Earth of 1.4×10^{-19} W/m^2, requires the use of large antennas with sensitive receivers. This 1.4×10^{-19} W/m^2 power density at Earth is from a spacecraft at a 5-AU distance with a 10-W transmitter and a directional antenna having a 50-dBi gain. For comparison, the noise power radiated by a room-temperature resistor in a 100-kHz bandwidth is 4×10^{-16} W, 2,857 times greater than the power received from the spacecraft by an antenna that has a 1 m^2 effective collecting area. Each current 34-m-diameter Deep Space Network (DSN) antenna has an effective collecting area of about 450 m^2 at 32 GHz, and the power received from the spacecraft (mentioned above) is about 1/6 the power from the room-temperature resistor in the 100-kHz bandwidth. The reception of modest data rates (100 kb/s) from such a spacecraft by the DSN requires sensitive receiving systems.

DSN receiving stations use antennas with large effective collecting areas and receivers with very low operating noise temperatures. Increasing the DSN receiving system antenna effective collecting area-to-system operating noise temperature ratio, A/T, can be done in a cost-effective way by minimizing the noise temperature of the first amplifier in the receiver. This is accomplished by the use of masers in the most sensitive DSN receiving systems.

The Jet Propulsion Laboratory's (JPL) experience with the development and use of masers for deep-space communications began in 1955 and spans a period of 45 years. Single-cavity, multiple-cavity, traveling-wave, and reflected-wave masers were developed and used in the DSN. All DSN low-noise masers

[1] Communications Ground Systems Section.

[2] Spacecraft Telecommunications Equipment Section.

use ruby as the active material. Ka-band maser research at JPL began with the evaluation of ruby as a maser material at frequencies between 26 GHz and 44 GHz [1] and with the construction of a reflected-wave maser [2] based on the successful design developed at K-band (19 GHz to 25 GHz) [3]. The reflected-wave maser offers wide instantaneous bandwidth (up to 500 MHz) and tuning ranges up to 6 GHz. The combination of wide instantaneous bandwidth and a large tuning range requires a large volume of ruby (2 to 4 cm^3) and considerable RF pump power (0.2 to 0.5 W). These requirements add to the expense of the maser and the difficulties of cooling the maser to the cryogenic temperatures below 5 K needed for best performance. Comb-type traveling-wave masers like those used in the DSN at 2.3 GHz (S-band) and 8.42 GHz (X-band) are very difficult to build at 32 GHz because the ruby slow-wave structure and distributed resonant isolators are very small, and the needed tolerances could not be achieved in an affordable way.

The ruby dual-cavity maser used for the Ka-band Link Experiment with the Mars Observer spacecraft (referred to as the KaBLE maser) [4,5] showed that cavity masers are a viable approach for achieving good noise performance and reasonable (80-MHz) instantaneous bandwidth, and they can be tunable for more than 500 MHz. The KaBLE maser was tested in the 34-m beam-waveguide antenna in a single-frequency listen-only configuration with the antenna at the zenith in cold, clear, dry weather. The system operating noise temperature, T_{op}, was measured as the maser was tuned from 33.68 GHz down to 33.06 GHz. A 28-K T_{op} was measured at 33.68 GHz, and the lower frequencies showed a steady improvement, reaching a 24.5-K T_{op} at 33.06 GHz. The KaBLE maser's performance was especially encouraging because there was not sufficient time to build a design that was optimized for maximum gain and bandwidth. Work on the design, construction, and installation of the maser was done in less than 1 year, the schedule being driven by the Mars Observer launch date.

The KaBLE maser required immersion in superfluid liquid helium, and the dewar required refilling several times a week. The liquid helium temperature was lowered to 1.5 K by reducing the pressure of the helium vapor to 0.005 atm.

A new 32-GHz cavity maser design is described here. The goals include (1) simplified DSN field operations, (2) high reliability with at least a 10,000-hour mean time between failure, (3) a tunable frequency range of at least 500 MHz with a maximized instantaneous bandwidth, (4) a minimized pump power requirement of less than 2 mW per cavity, and (5) a maser "module" noise temperature of approximately 3 K.[3]

The low pump power requirement will enable operation in a closed-cycle helium refrigerator (CCR) where the maser is operated in a vacuum and cooled by conduction to near 2 K. A commercially available 4-K Gifford–McMahon (GM) cycle CCR was modified for this purpose, and tests of the 2-K CCR are in progress.

II. Basic Design Philosophy

There are several approaches to cavity maser design. Early designs used relatively high quality factor (Q) microwave cavities [6]. This high-Q approach at L-band (960 MHz) and S-band frequencies yielded high gain, but the maser bandwidth was significantly less than the ruby linewidth. The reactance associated with the paramagnetic resonance was small compared with the cavity reactance. In this case, the ruby spin resonance can be modeled as a simple resistor, with weak frequency dependence. More generally, the spin resonance can be modeled as a parallel resonant circuit in series with a series resonant

[3] The "module" noise temperature is the complete amplifier noise temperature at the cryogenic input terminal to the amplifier. The module noise temperature does not include noise contributions from cryogenically cooled components or ambient components located between the amplifier and the interface to the antenna. This practice has been used to characterize high-electron mobility transistor (HEMT)-based amplifier modules and is used here to characterize the noise performance of this maser for comparative purposes.

circuit representing the cavity. Component values for the equivalent circuit shown in Fig. 1 are chosen to model the voltage gain-versus-frequency behavior for both the narrowband cavity maser and the spin resonance alone. The source impedance in the spin-only circuit is arbitrary, as the spins must exist in some sort of microwave structure. The circuits were analyzed using a commercially available software package named MMICAD [7]. In the narrowbandwidth maser, the entire bandwidth of the amplification response is essentially at the peak of the magnetic resonance line. Shifting the peak of the maser material spin resonance line by changing the applied magnetic field can be used to pull the center frequency of the amplified response to a frequency slightly above or below the center frequency of the high-Q microwave resonator.

Another approach is to broadband the single-cavity maser [8]. One may choose to broaden the resonant circuit associated with the ruby spins or the resonant circuit associated with the dielectric-filled cavity. Broadening the resonant circuit associated with the ruby spins leads to a broadening of the instantaneous bandwidth of the maser when the bandwidth of the dielectric-filled cavity is greater than the ruby linewidth. Broadening the resonant circuit associated with the dielectric-filled cavity leads to a broadening of the tunable bandwidth (tuning range) of the maser.

We consider first the spin-system broadening. The amplification bandwidth can exceed the ruby linewidth if the effects of the negative inductance (L) and capacitance (C) associated with the inverted spin system are compensated. This approach is referred to as "reactance compensation" [9]. An equivalent circuit representing this and its frequency response is shown in Fig. 2. It is noteworthy that the gain response of this circuit as analyzed is not simply a scaled inverted image of the spin system absorption response. This approach is essentially fixed frequency, eliminating any possibility of a tunable frequency range. Changing the magnetic field changes the resonant frequency of the spin system, and the amplification response is altered significantly, as shown in Fig. 3. Also, the adjustment of the reactance-compensated circuit is critical. A slight change in cavity loading can produce either a single narrow gain response or two sharp gain responses [10]. This approach was not chosen for our present design.

Alternatively, one may choose to broaden the dielectric-cavity response, making it much broader than the ruby linewidth. The KaBLE maser had a dielectric (ruby) resonator response that was broader than

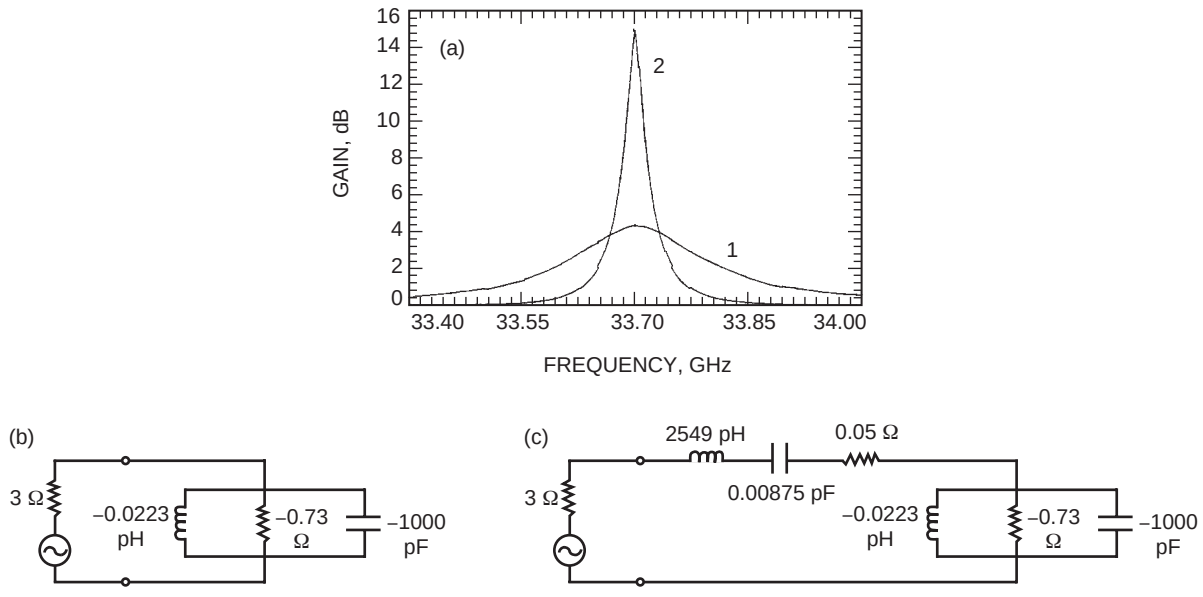

Fig. 1. Calculated gain curves (using MMICAD) of lumped-element circuits representing (a) the spin system only (curve 1) and a narrowband cavity maser (curve 2), (b) the equivalent circuit for curve 1, and (c) the equivalent circuit for curve 2.

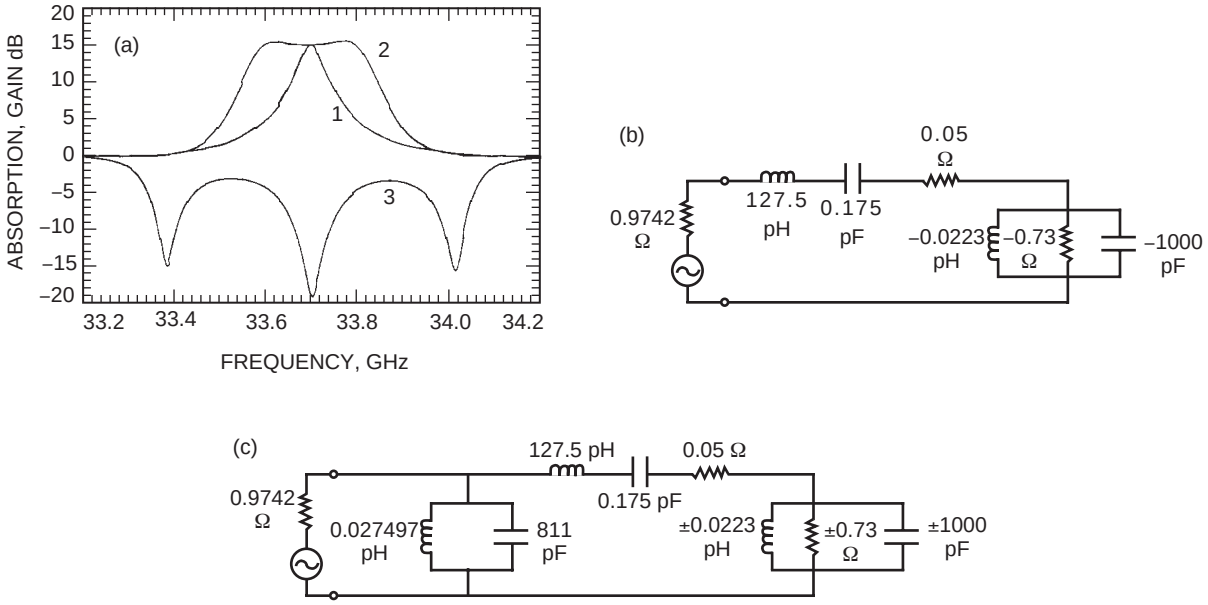

Fig. 2. Calculated gain curves (using MMICAD) of lumped-element circuits representing (a) a cavity containing a spin system (curve 1), that same cavity spin system broadbanded with an additional cavity and the spin system inverted (curve 2), and the spin system absorbing (curve 3), (b) the equivalent circuit for curve 1, and (c) the equivalent circuit for curves 2 and 3.

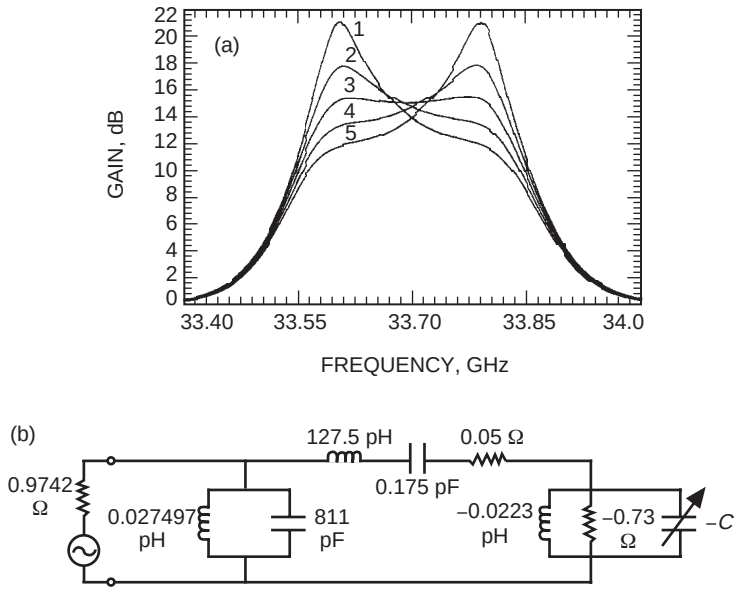

Fig. 3. Calculated gain curves (using MMICAD) of (a) the lumped-element circuit of Fig. 2 as the resonant frequency of the spin system is changed by varying the value of the negative capacitance, with curves 1 through 5 corresponding to capacitance values of −1001.0, −1000.5, −1000.0, −999.5, and −999.0 pF, respectively, and (b) the equivalent circuit.

the ruby linewidth, and the ruby's gain response could be tuned by changing the DC magnetic field and the pump frequency as shown in Fig. 4. However, the gain and bandwidth were not constant as the maser's center frequency was changed. Electronic control of the magnetic field shape, with trim coils near the rubies, traded bandwidth for gain so that adequate gain could be achieved across a 700-MHz range.

The present design will enable the ruby resonance to be tuned over more than 500 MHz within the cavity resonance (see Fig. 5). This is similar to the KaBLE maser, but the gain should not change with frequency. The cavity's amplitude response will be flat because the ruby-filled cavity is part of a critically coupled two-resonator pair with a flat amplitude response. The amplitude at the skirts (band edges) of the critically coupled pair will change more rapidly with frequency than those of a single resonator with the same Q.

Broadbanding the dielectric-cavity response causes the cavity maser to operate much like a traveling-wave maser (TWM). Tapering the magnetic field (to provide a broadened paramagnetic resonance) along the length of the ruby bars inhomogeneously broadens the ruby linewidth in a DSN TWM. The TWM's amplification response is shifted in frequency by changing the magnetic field and the pump frequencies, without retuning the slow-wave structure. The negative L and C (reactance) associated with the inverted spin system are not affected by the reactive components of the broad slow-wave structure response of the TWM. The present design will work in the same way, although the tapered magnetic field will be over a

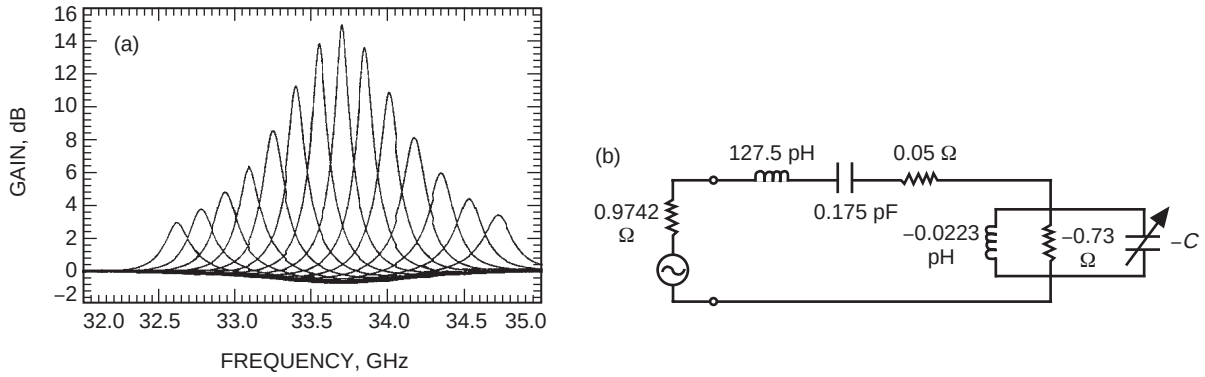

Fig. 4. Calculated gain curve (using MMICAD) of the single cavity containing (a) the spin system shown in Fig. 2 as the spin resonance is tuned through the cavity resonance by varying the negative capacitance, and (b) the equivalent circuit.

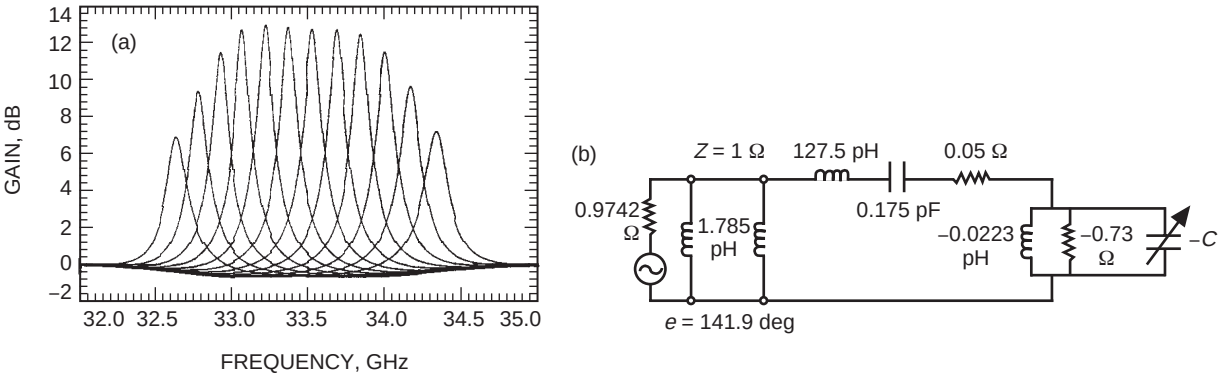

Fig. 5. Calculated gain curve (using MMICAD) of (a) the circuit in Fig. 4 with the addition of a cavity that broadbands the ruby-filled (dielectric) cavity as the spin system is tuned through the cavity resonance by varying the negative capacitance, and (b) the equivalent circuit.

very small piece of ruby, 0.1024 in. (2.601 mm) by 0.052 in. (1.321 mm) by 0.0396 in. (1.0058 mm), not a 3-in. (76.20 mm) or 6 in. (152.4 mm) ruby bar. Dimensions used for this cavity maser design, and used throughout this article, are in inches, with the metric equivalents given in parentheses. Waveguide designations (like WR-28) are identified based on dimensions in inches, and the commercial firm fabricating the parts work from drawings where all dimensions are given in inches. One inch equals 25.4 millimeters.

The gain of each cavity will be reduced to 13 dB or less by adjusting the slope or taper of the magnetic field across the ruby. Excellent gain stability is expected at modest gain levels of 13 dB or less. The instantaneous bandwidth of the amplified response increases as the gain of the cavity is reduced. A 300-MHz or greater instantaneous bandwidth can be achieved if the gain of each cavity is reduced to 5 or 6 dB. Five or six cavities in series should give a 30-dB net gain with a bandwidth of at least 300 MHz.

The noise temperature of the series of cascaded cavities acts much like the noise temperature of a TWM, being dependent on the bath temperature, the inversion ratio, and the gain-to-loss ratio. This is discussed in detail in a previous publication [5], where we find the noise temperature of a single cavity of the KaBLE maser to be 2.22 K, in accordance with

$$T_{amp} = \frac{G-1}{G}\,\frac{hf}{k}\left\{\frac{G_{\mathrm{edB}}}{G_{\mathrm{dB}}}\,\frac{r}{r-1} + \frac{L_{\mathrm{dB}}}{G_{\mathrm{dB}}}\,\frac{1}{e^{(hf/kT)}-1}\right\}$$

where G is the net power gain ratio, h is Planck's constant, f is the frequency, k is Boltzmann's constant, G_{edB} is the electronic gain in dB, G_{dB} is the net gain in dB, r is an inverted spin population ratio at the signal frequency, L_{dB} is the loss in dB, and T is the physical temperature (1.5 K in the case of the KaBLE maser).

The noise temperature of the KaBLE maser was calculated using an estimated cavity loss of 0.5 dB, a 13.5-dB net gain, and an inversion ratio of 2. If we assume the same loss and gain, and an inversion ratio of 1.7, in a helium bath at 2.2 K, the predicted noise temperature of a single cavity of the present design is 2.53 K. Adding a circulator with a 0.2-dB loss at 2.2 K increases the single-cavity noise temperature to 2.72 K. The $(G-1)/G$ term in the above equation becomes important when the cavity gain is reduced. The single-cavity noise temperature drops from 2.53 K to 2.12 K when the gain is reduced from 13.5 dB to 6 dB. The addition of the circulator gives an input noise temperature of 2.3 K. The effective noise temperature of a series of five cascaded cavities, each with a 5.8-dB gain, becomes

$$Te = 2.3 + \frac{2.3}{3.8} + \frac{2.3}{14.44} + \frac{2.3}{54.87} + \frac{2.3}{208.5} = 3.1\ \mathrm{K}$$

for a maser with a 29-dB net gain. This effective maser noise temperature at the input to the first circulator is defined as the maser module noise temperature. This should not be confused with the effective input noise temperature of the maser and feed system, which is expected to be about 5 K, the same as the KaBLE maser and feed package. Using a series of cavities of lesser gain per cavity to achieve a specified overall gain also improves the gain stability of the amplifier [4].

III. Ruby Cavity Design

There are several requirements for the ruby-filled cavity portion of the design. The cavity must be resonant at the signal frequency. In order to minimize the required RF pump power, the ruby-filled cavity is designed to be resonant at the pump frequency as well.

The volume of ruby is minimized through the use of a half-wavelength resonator (the KaBLE maser used a full-wavelength resonator). The volume of ruby used does not affect the strength of the maser

action, as the magnetic Q depends on the spin density and not the total number of spins. The output power level at which the maser begins to saturate is affected by the volume of ruby. It may be worth emphasizing that saturation in a maser due to large signals reduces the maser gain without producing intermodulation products. Maser-gain reduction begins to occur when the maser output signal reaches levels of about 0.1 μW (−40 dBm).

The magnetic field taper used to reduce the maser gain and increase the bandwidth will be done transverse to the direction of signal propagation because this is the long dimension of the ruby crystal in this design. (The KaBLE maser was tapered along the propagation direction, which was the long dimension of the crystal in that case.)

The filling factor of the ruby cavity is chosen to maximize the gain–bandwidth product. The signal is coupled to the ruby cavity from a resonant coupling cavity through a rectangular inductive iris or aperture. The resonant coupling cavity increases the electromagnetic field at the inductive iris, enabling the use of a smaller iris than would otherwise be used. The net effect of this technique is to trap the magnetic field lines of the stored energy in the cavity that is filled with ruby. This is in contrast with the KaBLE maser, where one whole side of the ruby was exposed to the signal waveguide. The filling factor of the KaBLE maser cavities were further reduced because the ruby was pulled out slightly into the WR-30 waveguide to increase the coupling to the ruby and lower the external Q.

The resonant frequency of a cavity that is partially filled with a dielectric material is determined by the dimensions of the cavity, the dielectric constant of the material that partially fills the cavity, and the dimensions and shape of the dielectric material within the cavity. The dielectric constant of ruby varies depending upon the relationship between the direction of the C-axis and the direction of the electric field within the ruby. The effective dielectric constant within the cavity can be adjusted by changing the volume of ruby. A small air gap (or vacuum gap) occurs on one side of the ruby by the application of pressure to one face of the ruby with a small, spring-loaded dielectric or metal rod. Consider a ruby with dimensions of 0.1024 in. (2.6010 mm) by 0.0508 in. (1.2903 mm) by 0.0396 in. (1.0058 mm) within a cavity having dimensions of 0.1032 in. (2.6213 mm) by 0.0512 in. (1.3005 mm) by 0.040 in. (1.016 mm). The volumetric filling factor is 97.5 percent. The electric field is perpendicular to the face of the ruby with 0.1024 in. (2.6010 mm) by 0.0508 in. (1.2903 mm) dimensions. The air gap of 0.0004 in. (0.01016 mm) exists between the cavity wall and this same face of the ruby.

Predicted values of the dielectric constant of ruby at 4 K are 11.2 parallel to the C-axis and 9.2 perpendicular to the C-axis [8]. The direction of the electric field of the stored signal energy in the cavity is at an angle of 54.7 deg to the ruby C-axis so the dielectric constant of the ruby-filled portion is expected to be around 10. The effective dielectric constant of the combination of the air gap and the ruby is calculated by considering the capacitance of two capacitors in series. The capacitors have equal areas, dielectric constants of 1 and 10, and a thickness of 0.01 mm and 1.006 mm, respectively. The equation for the total capacitance of two capacitors in series is used to find the total capacitance of the ruby and the air gap:

$$C_{\text{total}} = \frac{CrCa}{Cr + Ca}$$

The effective dielectric constant is determined using the individual capacitances expressed in terms of the thickness, t, and dielectric constant, ε, of each:

$$\varepsilon_{eff} = \frac{\varepsilon_r \varepsilon_a (t_r + t_a)}{\varepsilon_r t_a + \varepsilon_a t_r}$$

where ε_r and ε_a are the relative dielectric constants of ruby and air and t_r and t_a are the thicknesses of the ruby and air dielectrics. An air gap of 0.01 mm results in an effective dielectric constant of 9.18.

Alternatively, the effect of the air gap can be calculated using the formula for the change in resonant frequency of a cavity due to a material perturbation [11]. The values of the effective dielectric constants obtained by using the two different approaches are in close agreement.

The resonant frequencies of the cavity near 32 GHz (signal) and 66.4 GHz (pump) can be shifted in several ways. Changing the effective dielectric constant shifts the signal and pump resonant frequencies by about the same rate. Changing the width, 0.1024 in. (2.6010 mm), and the length, 0.0508 in. (1.2903 mm), of the cavity changes the signal and pump resonant frequencies at different rates. Plots of width and length combinations giving the desired signal and pump frequencies were used to determine the dimensions used in this design.

Directional transition probabilities [8] for the signal and pump transitions are used to ensure that the coupling between the ruby spin system and the signal and pump frequency stored energy is maximized. The ruby spin system is circularly polarized at the signal frequency and elliptically polarized at the pump frequency. The cavity uses resonant modes where the RF magnetic fields lie in a plane that is normal to the applied DC magnetic field used to give the needed Zeeman splitting.

The combination of the linear polarization of the RF field in the cavity and the circular polarization of the ruby spin system produces a maximum polarization filling factor of 50 percent. The 97.5 percent volume filling factor of this cavity and ruby arrangement and the 50 percent polarization filling factor produce a net overall filling factor of 0.4875. This value can be used with other cavity and ruby parameters to compute the gain and bandwidth that this design should provide. Expanding upon Siegman's [8] equation for the magnetic Q, Q_m, of a maser material and accounting for this new case, where hf is about the same as kT, we find

$$\frac{1}{Q_m} = \frac{2g^2\beta^2\mu_o}{h}\ \frac{I\Delta N\eta\sigma^2}{\Delta f_l} = (1.3)\left(10^{-18}\right)\frac{I\Delta N\eta\sigma^2}{\Delta f_l}$$

The equation gives a Q_m of ruby in the cavity described above, at 2.2 K, of about 18.9.

The midband voltage gain of a cavity maser can be determined by using another of Siegman's [8] equations:

$$G = \frac{\dfrac{1}{Q_e} + \dfrac{1}{Q_m}}{\dfrac{1}{Q_e} - \dfrac{1}{Q_m}}$$

where Q_e is the external Q, G is the voltage gain, and the power gain is G^2.

The design of the pair of critically coupled cavities for this maser gives a flat amplitude response of about 600 MHz with an external Q of 40. The cavity maser with the natural ruby linewidth of 60 MHz will oscillate because the maser material Q_m is much less than the cavity external Q. Broadening of the ruby linewidth with a tapered magnetic field will be used to raise the ruby's magnetic Q to give a gain of less than 13 dB. Increasing the ruby linewidth to 300 MHz increases the magnetic Q by a factor of five to 94.5. The resulting cavity gain will be 7.85 dB, with a cavity instantaneous bandwidth of about 240 MHz. Five cascaded cavity masers of the above design will give an instantaneous bandwidth covering 240 MHz with approximately 35 dB of net gain. The predicted results of trading gain for bandwidth for a single cavity are plotted in Fig. 6.

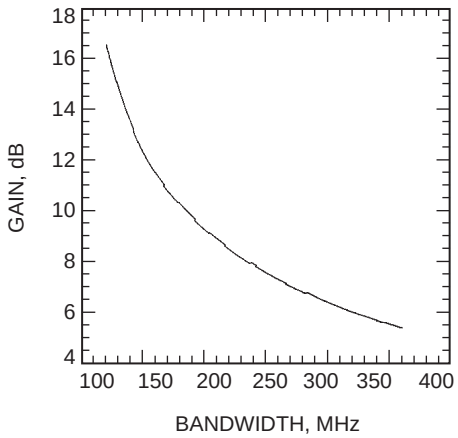

Fig. 6. Single-cavity gain versus bandwidth, assuming operation at 2.2 K with a ruby inversion ratio of 1.7.

IV. Signal Waveguide Circuit

The portion of the waveguide circuit discussed in this section includes the signal broadbanding cavity and the ruby cavity. The pump reject filter and the quarter-wave-matching transformers are basically transparent to the signal and will be covered in later sections. The signal circuit consists of a coupling cavity connected to the ruby-filled cavity with a relatively small iris. The coupling cavity serves two purposes. It acts as an impedance-matching transformer to couple from the WR-26 waveguide to the ruby-filled cavity to achieve the proper external Q, Q_e, and the coupling cavity also produces a flatter tuning response.

The impedance-matching action of the coupling cavity is necessary because of the large reflection of the signal in passing from the air-filled WR-26 to the ruby-filled cavity. The magnitude of the reflection coefficient at 32 GHz of this interface is 0.98. This is caused by the change in waveguide width, the thickness of the iris, and the change in wave impedance due to the dielectric constant of ruby. In order to couple the correct amount of signal into the ruby cavity, the field strength at the ruby aperture must be increased with the use of a resonant cavity.

The coupling cavity and the ruby cavity act as two nearly critically coupled cavities. Although this arrangement has about the same 3-dB bandwidth as a single cavity of the same Q, the bottom of the reflected response (measured in the reflection mode without pump power) is much flatter and the skirts are steeper. The flat frequency response is necessary in order to be able to tune the maser over 500 MHz without significant gain changes.

Thick inductive irises were chosen to form the resonant cavities. Thick irises are easier to machine and mechanically more stable than thin irises. Thick irises have the further advantage that, during the iterative design process, changing the length (also referred to as the thickness) of the iris will adjust the coupling to the cavity but have less effect on the resonant frequency than adjusting the iris aperture size. This can be important when the structure consists of many cavities in cascade and both signal and pump frequency responses are affected.

One disadvantage of thick inductive irises with small openings is the difficulty of deriving an equivalent circuit. The openings are small enough that the waveguide consisting of the iris itself is beyond cutoff. For example, the 0.142-in. (3.6068-mm) aperture with a length of 0.020 in. (0.5080 mm) has 2.45 dB of below-cutoff attenuation. The 0.060-in. (1.5240-mm) aperture with a length of 0.015 in. (0.3810 mm)

has 6.45 dB of below-cutoff attenuation. Figure 7 shows an equivalent circuit of the signal waveguide circuit and the calculated response using MMICAD. The bandwidth is larger than predicted using the mode-matching analysis program [12] because the equivalent circuit for the thick irises is approximate.

The electrical length, e, of the signal broadbanding cavity in Fig. 7 is 150 deg. The electrical length of the ruby cavity is 120 deg. This large deviation from 180 deg is partly due to the phase shift upon reflection from the below-cutoff waveguide opening at the pump end of the ruby cavity.

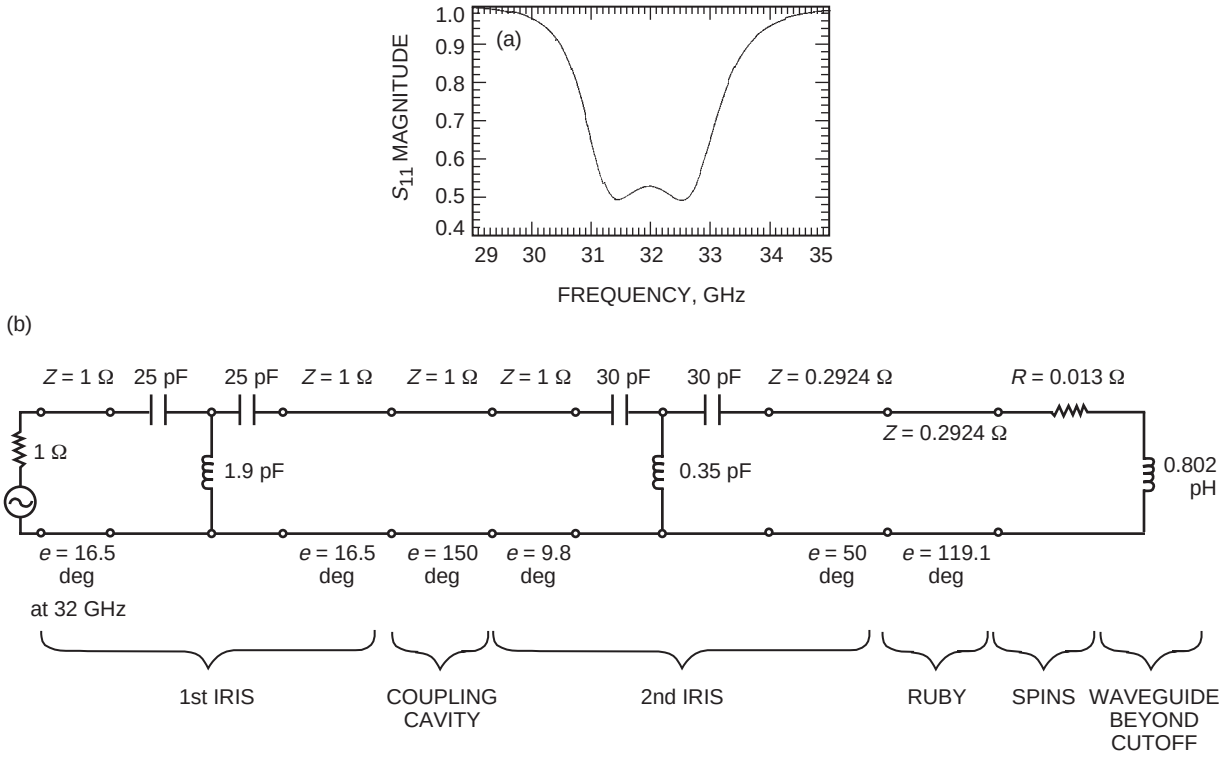

Fig. 7. Calculated response (using MMICAD) of (a) the transmission line lumped-element circuit representing the signal waveguide portion of the coupled cavity maser and (b) the equivalent circuit.

V. Pump Waveguide Circuit

The pump waveguide circuit is designed to efficiently couple RF pump energy from the pump source to the ruby cavity. A pump broadbanding cavity is used to impedance match from the pump waveguide (WR-13) to the ruby cavity, as well as to provide a flat response over a 1-GHz pump-tuning range.

The resonant mode in the ruby cavity at the pump frequency of 66.4 GHz is the TE_{301} mode. The resonant frequencies of several modes versus aperture size for the ruby cavity are shown in Fig. 8. The aperture size used for this maser is 0.060 in. (1.5240 mm). The cavity and iris dimensions were optimized using the mode-matching analysis program [12].

The TE_{102} mode resonance at 56.4 GHz and the TE_{501} mode resonance at 86.8 GHz have a significant effect upon the response of the cavity. The interaction of these modes causes a frequency response that does not look like a simple parallel resonant circuit. This is especially evident in the phase and amplitude response of S_{21}, as shown in Fig. 9. The additional complication of converting the pump energy from the TE_{10} mode in the empty pump-coupling cavity to the TE_{30} mode in the ruby cavity makes development of an equivalent circuit difficult.

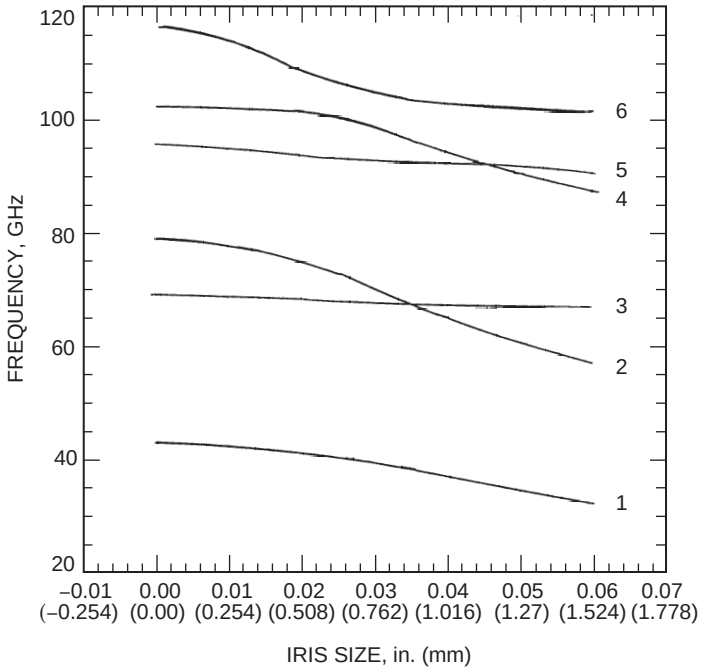

Fig. 8. Selected resonant frequencies of the ruby cavity versus iris size. Curves 1 through 6 represent the TE_{101}, TE_{102}, TE_{301}, TE_{501}, TE_{302}, and TE_{103} modes, respectively.

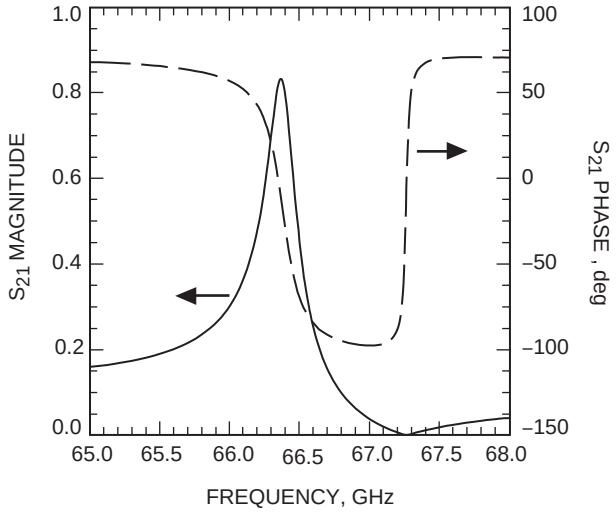

Fig. 9. Calculated magnitude and phase (using mode-matching analysis) of the forward scattering coefficient versus frequency for the ruby cavity at pump frequencies.

Some of the pump energy will also couple out of the cavity into the WR-26 waveguide. In order to redirect this energy back into the ruby cavity, a band-stop filter is located 0.4937 in. (12.54 mm) beyond the start of the signal broadbanding cavity. (The band-stop filter needs to be far enough away to ensure that evanescent modes do not interact with the 0.142 iris at signal wavelengths. Future masers may locate it closer.) This filter is essentially transparent at the signal frequency but is highly reflective at the pump frequency. A discussion of the filter is presented in Section VI. The location of this filter is arbitrary as far as the signal is concerned, but must be chosen properly for the pump energy. As a purely reactive reflector at the pump frequency, it has a significant effect on the response of the pump broadbanding cavity and the ruby cavity.

The waveguide TE_{mn} modes, where m is even, will be excited only if the irises are not symmetrically located about the centerline of the maser structure. We do not expect an appreciable amount of these modes to be excited. The filter does not offer much rejection to these modes. The modes where n is not zero are not excited in structures that use only inductive irises.

VI. Pump Reject Filter Design

The pump reject filter is used to confine the pump energy to the ruby-filled maser cavity and the adjacent signal and pump-coupling cavities. The intent of the pump reject filter is to minimize pump-energy radiation into the other components in the system and to further improve the pumping efficiency. A factor of almost two (1.95) improvement in pumping efficiency can be achieved by reflecting pump energy that is transmitted through the cavity into the signal waveguide back to the ruby cavity. Resonating the ruby cavity at the pump frequency and positioning the filter at the proper distance from the ruby cavity causes about 10 percent of the pump energy to be absorbed by the ruby spin system. This low value occurs because the pump transition probabilities near 66 GHz are very weak.

The pump frequency required for operation at 32 GHz is about 2.4-GHz higher than twice the signal frequency. Since the signal frequency has at least a 500-MHz tunable bandwidth, the pump frequency should cover approximately a 1-GHz bandwidth. Therefore, at 66.4 GHz, only about 1.5 percent bandwidth is necessary. This narrow bandwidth enables the use of a reflective band-stop filter with a narrow bandwidth, having more than 40-dB rejection from 65 GHz to 68 GHz for the TE_{10} dominant mode and low insertion loss at 32 GHz.

One approach that satisfies both requirements is a filter composed of a series of waveguides of different heights but equal widths. Two views of the filter structure are shown in Fig. 10. It has the further advantage of being relatively compact and easy to machine. It also was decided to use an asymmetrical structure, with the changes in height being in one direction. This simplifies the machining. The widths and heights of the waveguide also were chosen so the structure would be mechanically rigid.

At the pump frequency, the structure behaves like a series connection of parallel L–C circuits separated by one-quarter wavelength. The parallel L–C circuit is achieved by the use of a quarter-wavelength shorted waveguide. Lengths of waveguide provide the quarter-wavelength coupling. The actual lengths of the waveguide are not exactly 90 deg because of junction effects where the waveguides meet. A very good approximation to the performance can be achieved by modeling the steps in height as waveguide E-plane tees. An equivalent circuit of the entire filter structure is shown along with the MMICAD calculated response in Fig. 11. The waveguide E-plane tee equivalent circuit and the waveguide capacitive step equivalent circuit were calculated from data in [13]. The filter was originally designed, and the final dimensions of the filter were optimized, using the mode-matching analysis program referenced previously.

The reflective behavior of the filter was calculated with the mode-matching program. The result is shown in Fig. 12. As can be seen, the filter is reflective rather than dissipative. This excellent rejection at 66.4 GHz is only for the TE_{10} mode. The rejection of the TE_{20} mode is minimal, but we do not anticipate a large amount of this mode to be excited due to the symmetry of the remainder of the maser structure.

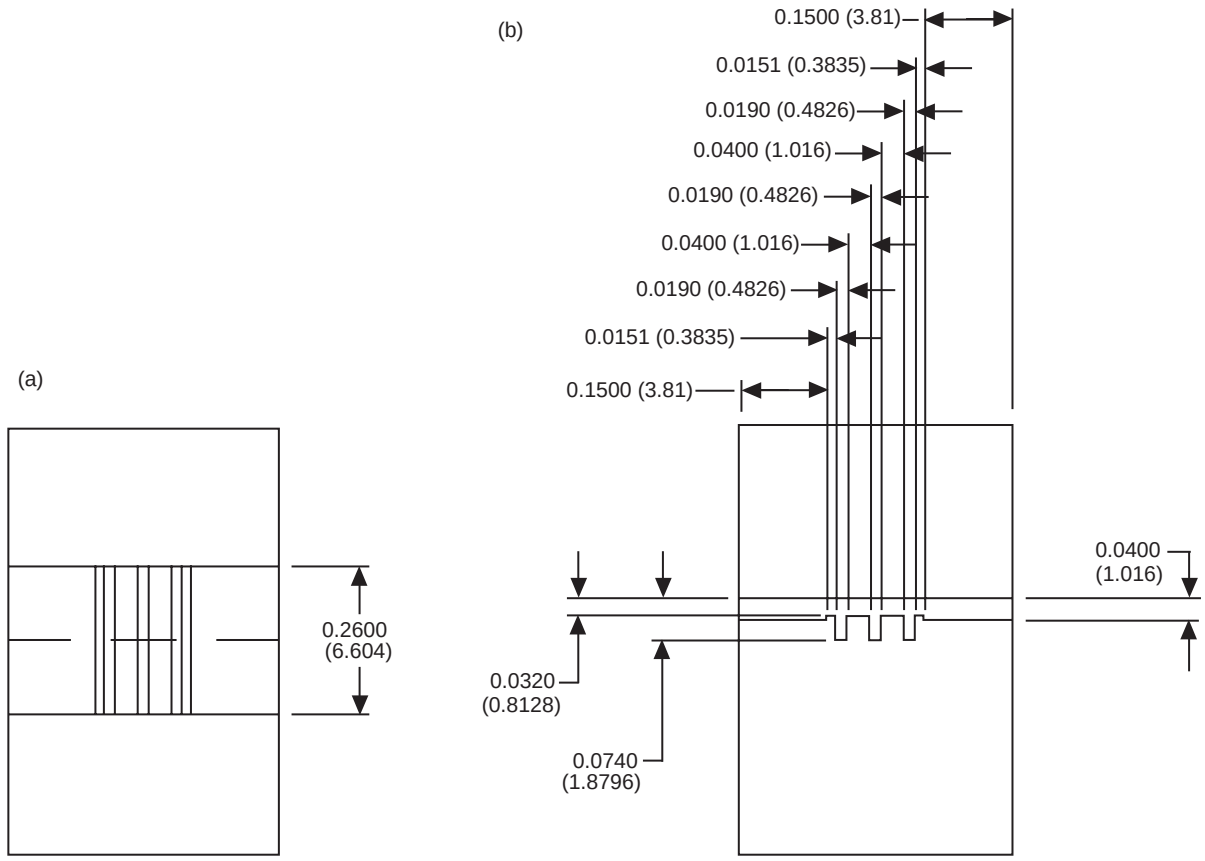

Fig. 10. The pump reject filter: (a) top view and (b) side view. (Dimensions are given in inches with millimeters in parentheses.)

VII. Quarter-Wave Transformers

The construction of the maser cavity in reduced-height and reduced-width waveguide necessitates the use of impedance-matching transformers to transition from standard waveguide sizes. The signal waveguide-matching transformer is from 0.280 in. (7.112 mm)-by-0.140 in. (3.556 mm) waveguide (WR-28) to 0.260 in (6.604 mm)-by-0.040 in. (1.016 mm) waveguide. The pump waveguide-matching transformer is from 0.148 in. (3.7592 mm)-by-0.074 in. (1.8796 mm) waveguide (WR-15) to 0.130 in. (3.302 mm)-by-0.040 in. (1.016 mm) waveguide. One standard approach is to use quarter-wavelength sections of intermediate impedance waveguide.

The quarter-wave transformers were designed using the principle that the intermediate-section impedance should be the geometric mean of the end impedances. This can be repeated if several matching sections are desired. The transformer sections are constructed such that one wall is common. This simplifies the machining of the structure.

Two intermediate steps were chosen for the signal waveguide. The guide dimensions of the first step are 0.275 in. (6.985 mm) by 0.102 in. (2.5908 mm) by 0.116 in. (2.9464 mm). The guide dimensions of the second step are 0.265 in. (6.7310 mm) by 0.055 in. (1.3970 mm) by 0.116 in. (2.9464 mm). The calculated return loss is shown in Fig. 13. It is better than 40 dB from 30.15 GHz to 33.7 GHz.

Two intermediate steps also were chosen for the pump waveguide. The guide dimensions of the first step are 0.143 in. (3.6322 mm) by 0.063 in. (1.6002 mm) by 0.0573 in. (1.4554 mm). The guide dimensions

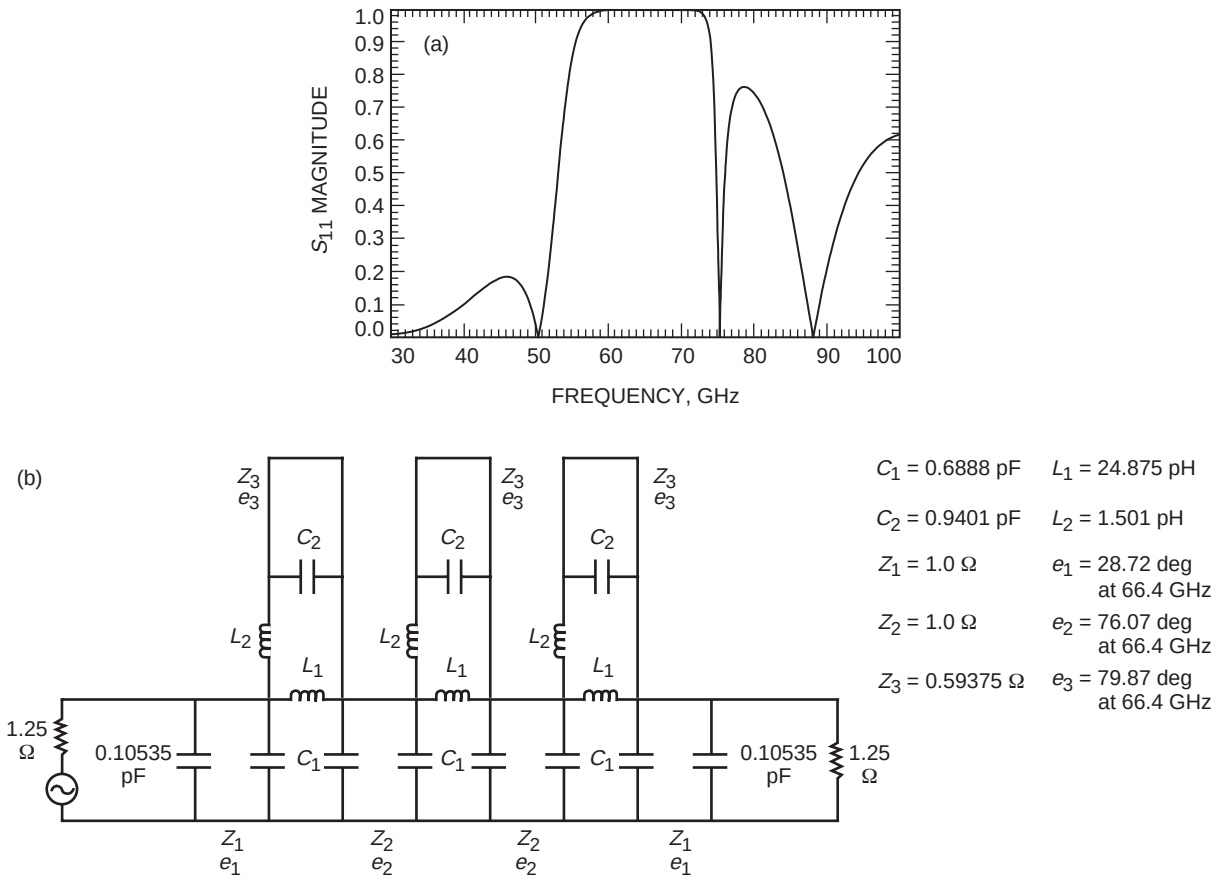

Fig. 11. Calculated (using MMICAD) (a) reverse scattering coefficient amplitude response for the pump reject filter and (b) the transmission line equivalent circuit.

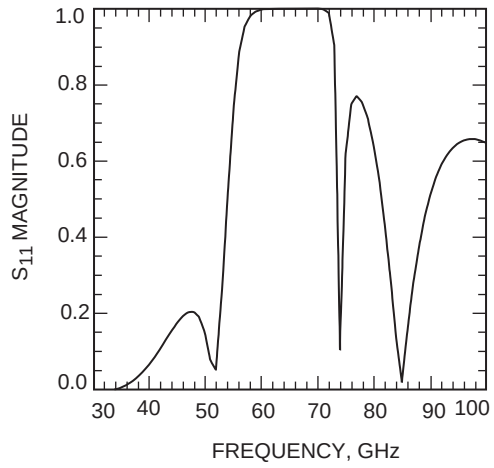

Fig. 12. Calculated reverse scattering coefficient amplitude response (using mode-matching analysis) for the pump reject filter.

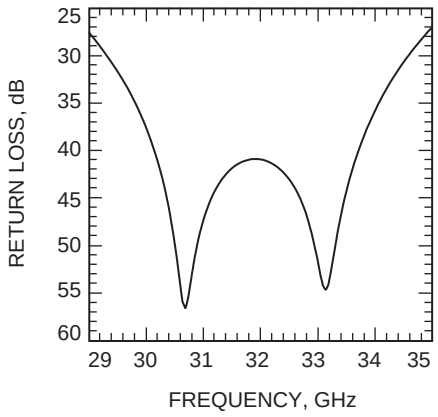

Fig. 13. Calculated return loss (using mode-matching analysis) of the signal waveguide quarter-wave transformer matching network.

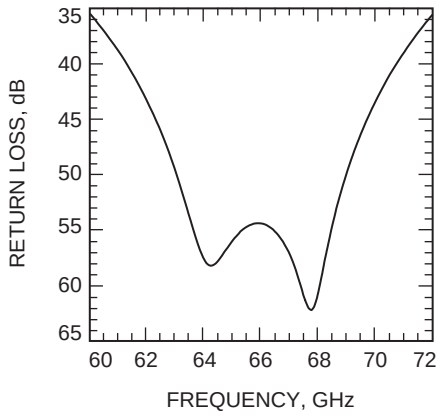

Fig. 14. Calculated return loss (using mode-matching analysis) of the pump waveguide quarter-wave transformer matching network.

of the second step are 0.136 in. (3.4544 mm) by 0.047 in. (1.1938 mm) by 0.056 in. (1.4224 mm). The calculated return loss is shown in Fig. 14. It is better than 40 dB from 61.3 GHz to 70.7 GHz. The return loss at 66.4 GHz is 54.9 dB.

VIII. Predicted Performance

The complete maser interior dimensions are shown in Table 1. Top- and side-view drawings of the maser are shown in Fig. 15. It is designed to mate to a WR-28 waveguide on one end and a WR-15 waveguide on the other end. The maser is composed of 21 sections. Sections 1 and 2 comprise the signal quarter-wave transformer. Section 3 is a section of reduced-height WR-26 to provide separation between the transformer junctions and the pump band-stop filter. Sections 4 through 10 comprise the band-stop filter. Section 11 is another section of reduced-height WR-26 to provide separation between the filter and the signal broadbanding cavity. Section 12 is the first iris of the signal broadbanding cavity. Section 13 is the interior of the cavity. Section 14 is an iris between the signal broadbanding cavity and the ruby cavity. Section 15 is the interior of the ruby cavity. Section 16 is the iris between the pump broadbanding cavity and the ruby cavity. Section 17 is the interior of the pump broadbanding cavity. Section 18 is the second iris of the pump broadbanding cavity. Section 19 is a section of reduced-height WR-13 to provide separation between the pump broadbanding cavity and the pump quarter-wave transformer. Sections 20 and 21 comprise the pump quarter-wave transformer.

The total length of the maser is 1.70 in. (43.18 mm). As mentioned previously, a significant portion of this is the 0.4937 in. (12.54 mm) of reduced-height WR-26 between the pump band-stop filter and the signal broadbanding cavity. Computer simulations suggest that this length can be shortened. For this first test structure, we have chosen this length of waveguide to minimize the risk of unpredictable interactions that might be caused by evanescent modes.

The calculated response of this structure using the rectangular waveguide mode-matching program is shown in Figs. 16 and 17. Figure 16 is the return loss looking into the signal waveguide. Previous measurements of cavity loss in the KaBLE maser showed no measurable copper losses at temperatures below 5 K. The resistivity of copper is reduced significantly at cryogenic temperatures as compared with the room-temperature resistivity. The waveguide is assumed lossless, but the loss tangent of the ruby filling the ruby cavity has been adjusted artificially to give approximately 6 dB of absorption. This signal absorption is physically caused by the ruby spin system when there is no pump power applied. This

Table 1. Width, height, and length of the waveguide sections of Fig. 15.

Width, in. (mm)	Height, in. (mm)	Length, in. (mm)
0.2750 (6.9850)	0.102 (2.5908)	0.1160 (2.9464)
0.2650 (6.7310)	0.055 (1.3970)	0.1160 (2.9464)
0.2600 (6.6040)	0.040 (1.0160)	0.1500 (3.8100)
0.2600 (6.6040)	0.032 (0.8128)	0.0151 (0.3835)
0.2600 (6.6040)	0.074 (1.8796)	0.0190 (0.4826)
0.2600 (6.6040)	0.032 (0.8128)	0.0400 (1.0160)
0.02600 (6.6040)	0.074 (1.8796)	0.0190 (0.4826)
0.2600 (6.6040)	0.032 (0.8128)	0.0400 (1.0160)
0.2600 (6.6040)	0.074 (1.8796)	0.0190 (0.4826)
0.2600 (6.6040)	0.032 (0.8128)	0.0151 (0.3835)
0.2600 (6.6040)	0.040 (1.0160)	0.4937 (12.5400)
0.1420 (3.6068)	0.040 (1.0160)	0.0200 (0.5080)
0.2600 (6.6040)	0.040 (1.0160)	0.2185 (5.5499)
0.0600 (1.5240)	0.040 (1.0160)	0.0150 (0.3810)
0.1032 (2.6213)	0.040 (1.0160)	0.0512 (1.3005)
0.0600 (1.5240)	0.040 (1.0160)	0.0200 (0.5080)
0.1300 (3.3020)	0.040 (1.0160)	0.0956 (2.4282)
0.0700 (1.7780)	0.040 (1.0160)	0.0200 (0.5080)
0.1300 (3.3020)	0.040 (1.0160)	0.1000 (2.5400)
0.1360 (3.4544)	0.047 (1.1938)	0.0560 (1.4224)
0.1430 (3.6322)	0.063 (1.6002)	0.0573 (1.4554)

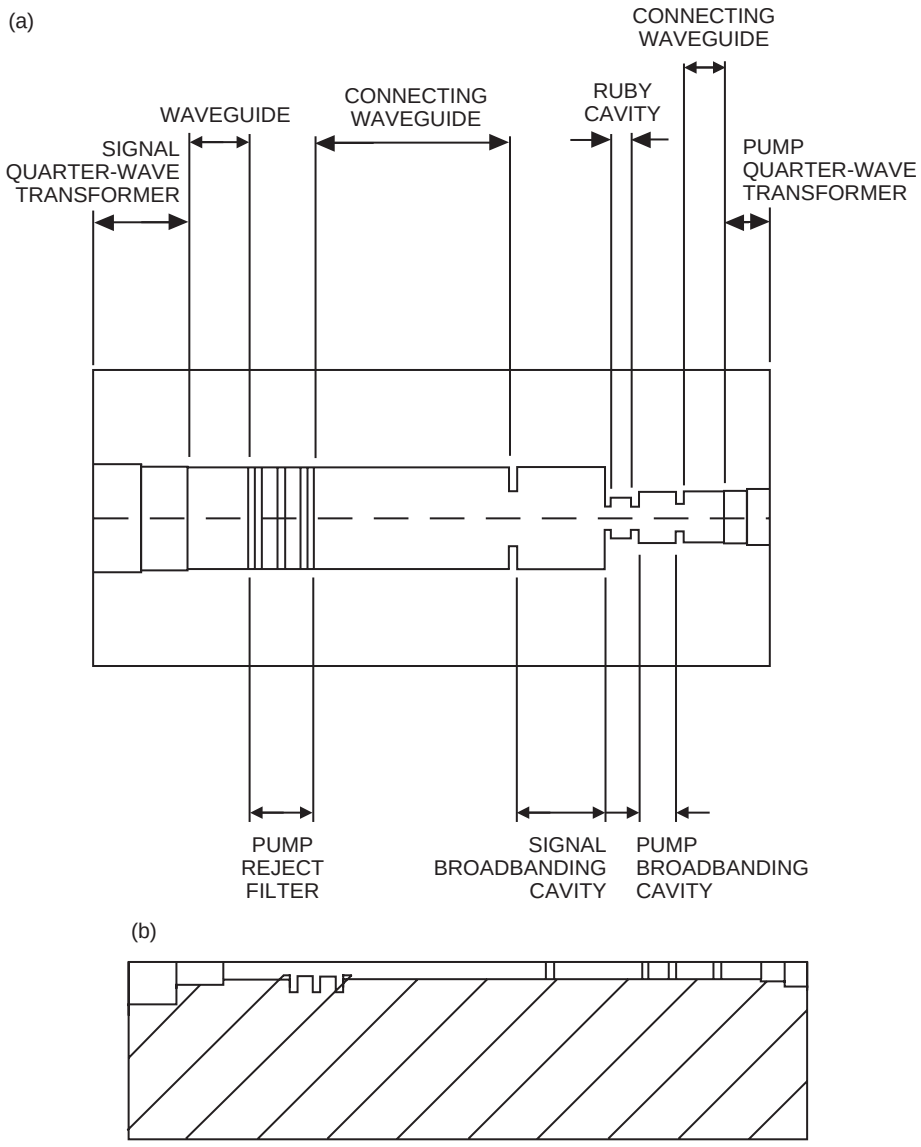

Fig. 15. The complete coupled cavity maser structure: (a) top view and (b) side view.

band corresponds to a maser electronic gain of 10.2 dB, assuming an inversion ratio of 1.7. The instantaneouswidth will not be the 700 MHz shown in Fig. 16. The magnetic field staggering over the ruby will be adjusted to give 6 dB of absorption. Figure 16 indicates the envelope of the ruby signal absorption as the magnetic resonance frequency is changed by varying the applied DC magnetic field.

Figure 17 shows the return loss looking into the pump waveguide. The waveguide again is assumed lossless. The value of the dielectric loss tangent used for modeling the absorption at the pump frequency was estimated from the ratio of the signal transition probability to the pump transition probability. The return loss is about 0.45 dB (corresponding to a power absorption of approximately 10 percent) from 65.8 GHz to 67.0 GHz. Figure 17 also indicates the envelope of the ruby pump absorption as the magnetic resonance frequency is changed with the magnetic field.

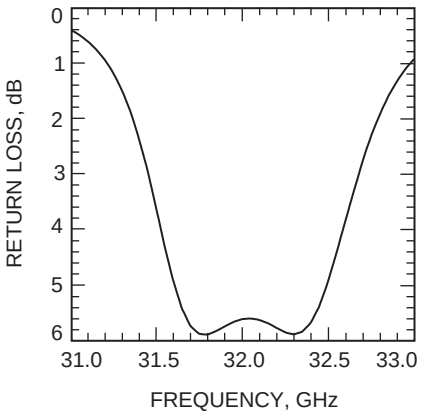

Fig. 16. Calculated return loss (using mode-matching analysis) looking into the signal port of the maser (without the quarter-wave transformers).

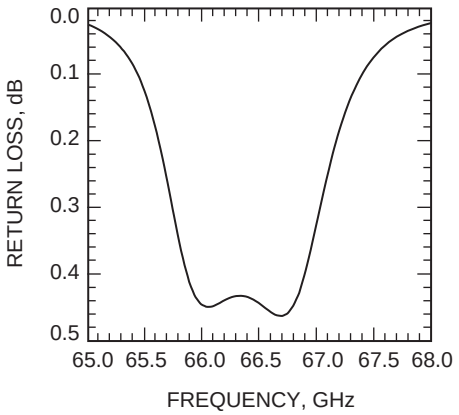

Fig. 17. Calculated return loss (using mode-matching analysis) looking into the pump port of the maser (without the quarter-wave transformers).

IX. Future Improvements

There are a number of geometries that extend the basic maser cavity design described in this article. They may prove suitable for a second- or third-generation maser after the present cavity design has been demonstrated. The first three geometries are devoted to decreasing the length of the maser. This is important in terms of fitting multiple cavities into a small superconducting magnet. The performance will not be substantially different from the maser described in this article. The last two geometries are devoted to increasing the performance of the maser.

One simple way to reduce the size of the maser is to decrease the spacing between the pump band-stop filter and the signal broadbanding cavity. In the current design, this distance is 0.4937 in. (12.54 mm), or 29 percent of the total length. If the filter is too close to the broadbanding iris, there will be interactions between them. Almost certainly the filter can be moved closer if the dimensions are properly adjusted.

Since the band-stop filter is essentially transparent at signal frequencies, it may be possible to extend the size of the broadbanding cavity and place the filter inside. Alternatively, one could decrease the number of resonant elements in the band-stop filter and keep the cavity smaller. For the present design, we have chosen to use empty broadbanding cavities to allow for the use of tuning slugs.

Another reduction in length may be possible by removing the quarter-wave transformers on both the signal waveguide and pump waveguide and adjusting the apertures of the irises accordingly. However, this makes the tolerances of the cavity dimensions even tighter.

If a larger tuning range is desired, one can add another signal broadbanding cavity. The pump band-stop filter can be located in front of both broadbanding cavities or placed inside one of them. Figure 18 shows a geometry where there are two broadbanding cavities. The internal dimensions are given in Table 2. The return loss looking into the signal waveguide is shown in Fig. 19.

If a larger gain–bandwidth product is desired, it may be possible to use two ruby cavities adjacent to one another. The pumping is more involved, but it is an efficient use of pump power. The power absorbed by one cavity is a small percentage of the incident power because the pump transition probabilities are small. There should be adequate pump energy emerging from the first cavity to allow inversion of the ruby in the second cavity. A possible geometry is shown in Fig. 20. The internal dimensions are given in Table 3. The return loss looking into the signal waveguide is shown in Fig. 21.

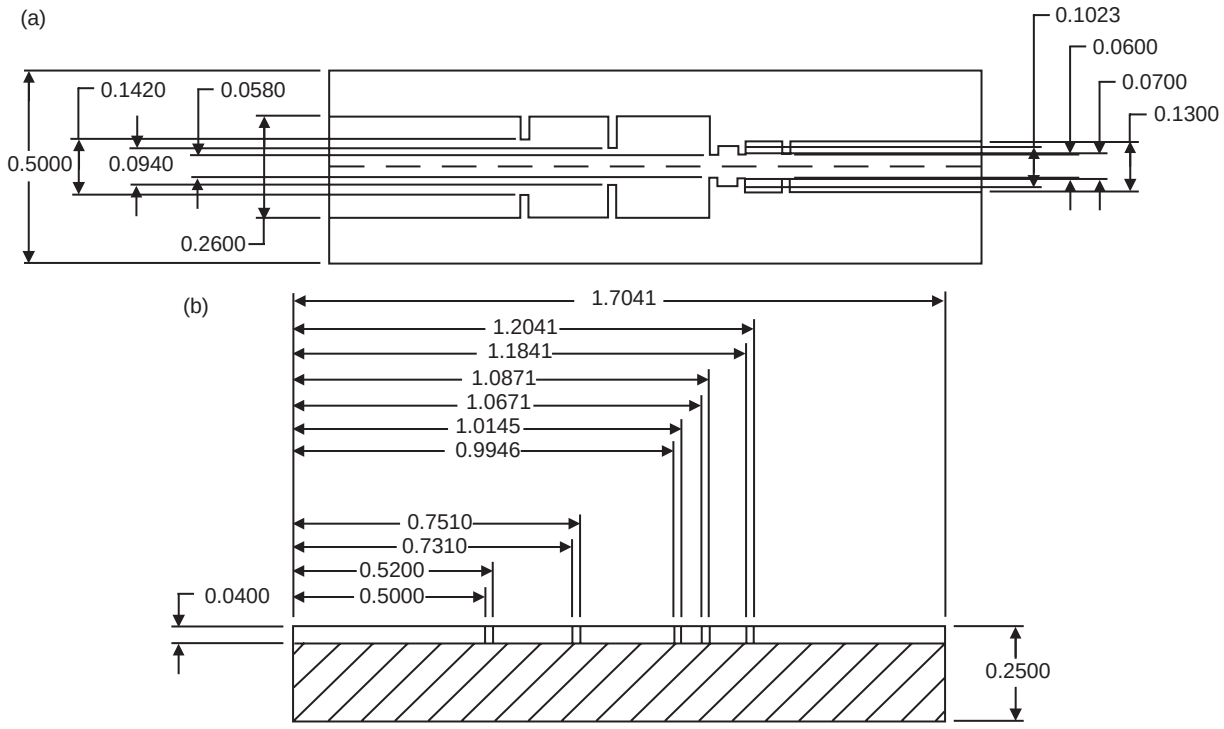

Fig. 18. A maser with two broadbanding cavities for the ruby-filled cavity: (a) top view and (b) side view. (Dimensions are in inches. For metric dimensions, see Table 2.)

Table 2. Width, height, and length of the waveguide sections of Fig. 18.

Width, in. (mm)	Height, in. (mm)	Length, in. (mm)
0.2600 (6.6040)	0.040 (1.0160)	0.5000 (12.700)
0.1420 (3.6068)	0.040 (1.0160)	0.0200 (0.5080)
0.2600 (6.6040)	0.040 (1.0160)	0.2110 (5.3594)
0.0940 (2.3876)	0.040 (1.0160)	0.0200 (0.5080)
0.2600 (6.6040)	0.040 (1.0160)	0.2435 (6.1849)
0.0580 (1.4732)	0.040 (1.0160)	0.0200 (0.5080)
0.1023 (2.5984)	0.040 (1.0160)	0.0526 (1.360)
0.0600 (1.5240)	0.040 (1.0160)	0.0200 (0.5080)
0.1300 (3.3020)	0.040 (1.0160)	0.0970 (2.4638)
0.0700 (1.7780)	0.040 (1.0160)	0.0200 (0.5080)
0.1300 (3.3020)	0.040 (1.0160)	0.5000 (12.700)

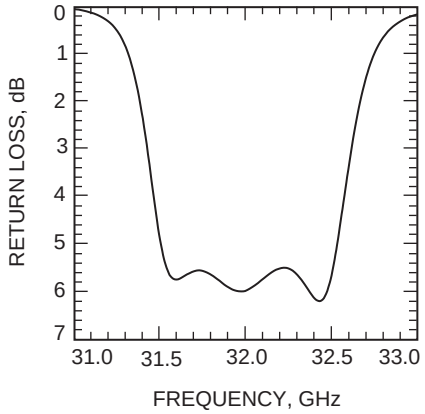

Fig. 19. Calculated return loss (using mode-matching analysis) looking into the signal waveguide of the structure in Fig. 18.

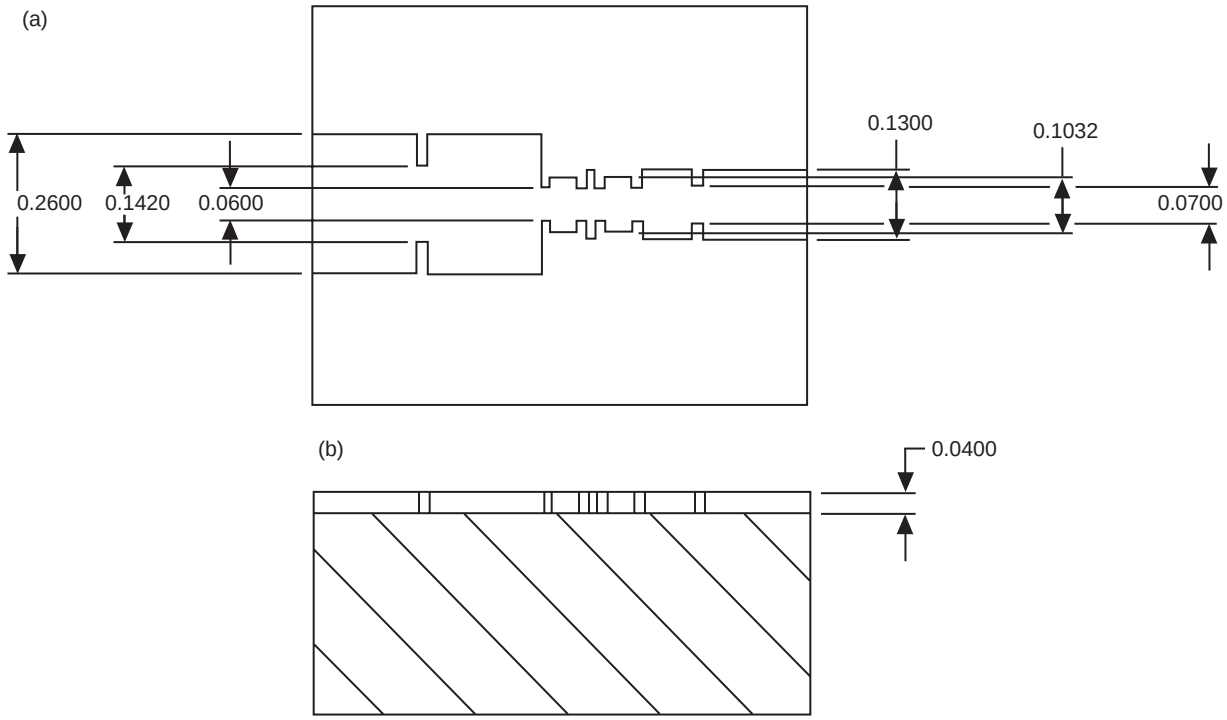

Fig. 20. A maser with two ruby cavities and one broadbanding cavity: (a) top view and (b) side view. (Dimensions are in inches. For metric dimensions, see Table 3.)

X. Conclusion

A 32-GHz coupled-cavity maser has been designed. It will be tunable over the 500-MHz deep-space allocation. It was designed to operate in a 2.2-K closed-cycle refrigerator (CCR) to simplify DSN field operations. The predicted noise temperature in the 2.2-K CCR is 3.1 K. The plan is to build and test the maser microwave cavity in the summer of 2000.

Table 3. Width, height, and length of the waveguide sections of Fig. 20.

Width, in. (mm)	Height, in. (mm)	Length, in. (mm)
0.2600 (6.6040)	0.040 (1.0160)	0.2000 (5.0800)
0.1420 (3.6068)	0.040 (1.0160)	0.0200 (0.5080)
0.2600 (6.6040)	0.040 (1.0160)	0.2184 (5.5474)
0.0600 (1.5240)	0.040 (1.0160)	0.0150 (0.3810)
0.1032 (2.6213)	0.040 (1.0160)	0.0514 (1.3056)
0.0600 (1.5240)	0.040 (1.0160)	0.0190 (0.4826)
0.1300 (3.3020)	0.040 (1.0160)	0.0160 (0.4064)
0.0600 (1.5240)	0.040 (1.0160)	0.0190 (0.4826)
0.1032 (2.6213)	0.040 (1.0160)	0.0517 (1.3132)
0.0600 (1.5240)	0.040 (1.0160)	0.0190 (0.4826)
0.1300 (3.3020)	0.040 (1.0160)	0.0956 (2.4282)
0.070 (1.7780)	0.040 (1.0160)	0.0200 (0.5080)
0.1300 (3.3020)	0.040 (1.0160)	0.2000 (5.0800)

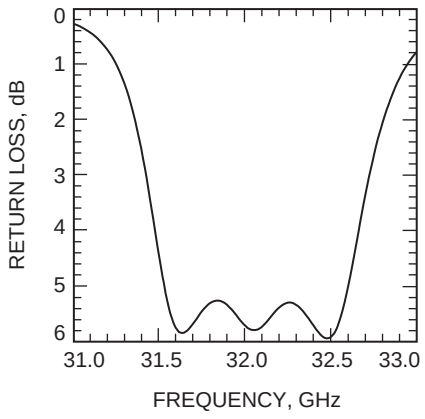

Fig. 21. Calculated return loss (using mode-matching analysis) looking into the signal waveguide of the structure in Fig. 20.

Acknowledgments

The authors would like to thank Dan Hoppe for useful discussions and for providing the rectangular waveguide (with dielectric) mode-matching program. Thanks also to Rex Quinn for preparing drawings.

References

[1] C. R. Moore and D. Neff, "Experimental Evaluation of a Ruby Maser at 43 GHz," *IEEE Trans.*, vol. MTT 30, pp. 2013–2015, 1982.

[2] J. Shell and D. Neff, "A 32-GHz Reflected-Wave Maser Amplifier With Wide Instantaneous Bandwidth," *The Telecommunications and Data Acquisition Progress Report 42-94, April–June 1988*, Jet Propulsion Laboratory, Pasadena, California, pp. 145–162, August 15, 1988.
http://tmo.jpl.nasa.gov/tmo/progress_report/42-94/94L.PDF

[3] C. R. Moore and R. C. Clauss, "A Reflected-Wave Ruby Maser with K-band Tuning Range and Large Instantaneous Bandwidth," *IEEE Trans.*, vol. MTT-27, pp. 249–256, 1979.

[4] J. Shell and R. B. Quinn, "A Dual-Cavity Ruby Maser for the Ka-Band Link Experiment," *The Telecommunications and Data Acquisition Progress Report 42-116, October–December 1993*, Jet Propulsion Laboratory, Pasadena, California, pp. 53–70, February 15, 1994.
http://tmo.jpl.nasa.gov/tmo/progress_report/42-116/116f.pdf

[5] J. S. Shell, R. C. Clauss, S. M. Petty, G. W. Glass, M. S. Fiore, J. J. Kovatch, J. R. Loreman, D. E. Neff, R. B. Quinn, and D. L. Trowbridge,"Ruby Masers for Maximum G/T_{op}," *Proceedings of the IEEE*, vol. 82, no. 5, pp. 796–810, May 1994.

[6] W. H. Higa and R. C. Clauss, "Dual-Cavity Maser Used in Mars Radar Experiment," *Proceedings of the IEEE*, vol. 51, no. 6, p. 948, June 1963.

[7] *MMICAD for Windows*, Version 2, Optotek Ltd., Kanata, Ontario, Canada, 1993–1996.

[8] A. E. Siegman, *Microwave Solid State Masers*, New York: McGraw-Hill Book Company, 1964.

[9] W. J. Getsinger, "Prototypes for Use in Broadbanding Reflection Amplifiers," *IEEE Transactions on Microwave Theory and Techniques*, vol. 11, pp. 486–497, November 1963.

[10] R. L. Kyhl, R. A. McFarlane, and M. W. P. Strandberg, "Negative L and C in Solid State Masers," *Proceedings of the IRE*, vol. 50, pp. 1608–1623, July 1962.

[11] R. F. Harrington, *Time-Harmonic Electromagnetic Fields*, New York: McGraw-Hill Book Company, 1961.

[12] D. J. Hoppe, "Modal Analysis Applied to Circular, Rectangular, and Coaxial Waveguides," *The Telecommunications and Data Acquisition Progress Report 42-95, July–September 1988*, Jet Propulsion Laboratory, Pasadena, California, pp. 89–96, November 15, 1988.
http://tmo.jpl.nasa.gov/tmo/progress_report/42-95/95I.PDF

[13] N. Marcuvitz, *Waveguide Handbook*, London: Peter Peregrinus Ltd., 1986.